Sulfonated graphene – An efficient cationic dye adsorbent in aqueous solution

Smriti Arora, Ritika Nagpal, Sweta Mishra, SMS Chauhan[*]

Bioorganic Laboratory, Department of Chemistry, University of Delhi, Delhi 110 007, India

[*]Corresponding author; Tel: (+91) 11-27666845; Fax: (+91) 11-27666605; E-mail: smschauhan@chemistry.du.ac.in

Abstract

A fast, sensitive, label-free, and organic cationic dye adsorbent has been developed by hydrothermal sulfonation reaction on reduced graphene oxide. The layered graphene sheet provides a significant surface area, high intrinsic mobility while presence of $-SO_3H$ groups on both sides of sheet render strong hydrophilicity and good dispersibility in water. The dye adsorption process is followed using UV–Visible spectroscopy, while the material before and after adsorption has been characterized by Raman, Powder XRD, FT-IR, TGA, TEM, SEM analysis. Optimum experimental parameters were determined to be acidic for Rhodamine B (RB) and basic for Methylene Blue (MB), temperature 30°C, adsorbent dosage 50 mg/L. The sorption equilibrium data were modeled using various isotherms, where the data best fitted to Freundlich isotherm for RB (q_{max} = 76.68 mg/g), while Langmuir isotherm for MB (q_{max} = 564.97 mg/g). The results indicate that the heterogeneous adsorbent can be applied for efficient dye removal from industrial effluent and contaminated natural water. Copyright © 2017 VBRI Press.

Keywords: Sulfonated reduced graphene oxide, rhodamine B, methylene blue, methyl orange, waste water treatment.

Introduction

Wastewater discharged from industries based on textiles, paper, leather, food, and cosmetics pose a serious threat to water bodies as they use high concentration of dye stuff. Dyes being complex aromatic molecules have poor biodegradability, and most of the dyes have mutagenic or carcinogenic effect on human as well as aquatic life [1]. Hence, there is an urge to develop novel, cost effective, and efficient materials for the removal of contaminants in water. Various methods including adsorption, coagulation, precipitation, ion exchange, filtration, and membrane separation are generally used in the removal of dyes from wastewater [2]. The materials used in these processes include rice husk [3], activated carbon [4], orange peel [5], neem leaf [6], red mud [7], bagasse fly ash [8], sawdust [9], conducting polymers [10], etc.

Activated carbon is a material of choice usually employed by the industries to reduce effluent waste [11] when adsorption based technique is considered. Graphene, a carbon-based material, where atoms are closely packed into honeycomb two-dimensional (2D) lattice has attracted considerable attention world over due to its excellent physiochemical and mechanical properties, which can be varied easily by its chemical functionalization. Owing to its potential properties, graphene has been used as a promising candidate for several applications such as sensors, solar cells, field-effect transistors, supercapacitors and transparent electrodes [12]. Infact, functionalized graphene being a carbon based layered structure have been presented as an efficient adsorbent [13].

Recently, many research groups have reported the adsorption behavior of oxidized and reduced forms of graphene[14]. Chemically oxidized form of graphite consists of sheets decorated with hydroxyl, epoxy groups at the basal plane and carboxyl groups at the sheet edges. These functional groups can interact with positively charged species like metal ions [15], biomolecules [16], polymers [17], and act as weak acid cation exchange resin which allow ion exchange with metal cations or positively charged organic molecules such as cationic dyes [18]. Therefore, graphene based materials have proven to be an effective adsorbent for removal of dyes from wastewater [19,20].

Earlier, our group has studied the catalytic properties of sulfonated form of graphene for the synthesis of expanded porphyrins [21]. The present studies explore the possibility of using sulfonated reduced graphene oxide (rGO-SO_3H) for dye removal from aqueous solutions. Adsorption studies have been reported using graphene oxide, its reduced form and its hybrid with different metal ions [22] but till date no report has been presented on sulfonated form of graphene. The sulfonic group posses' high negative charge as compared to hydroxyl and carboxyl groups of graphene oxide, therefore, the cationic dyes are expected to bind more effectively. Methylene Blue, Rhodamine B have been chosen as the cationic adsorbate, and Methyl orange, as an anionic adsorbate. The dye/adsorbent interactions have been investigated in detail in this paper by FT-IR, Raman, TEM analysis.

Experimental

Materials

Graphite powder (325 mesh, 99.99% purity) was obtained from Alfa Aesar, USA, Sodium nitrite (NaNO$_3$) 98% purity; Potassium Permanganate (KMnO$_4$) of 97% purity, Sodium Borohydride (NaBH$_4$) ~ 98%, Sulfuric Acid (H$_2$SO$_4$) ~ 95-98%, Rhodamine B (RB) with dye content of 95%, Methyl Orange (MO) with dye content of 85%, Methylene Blue (MB) with dye content $\geq$ 85% and fuming sulfuric acid 65.5-68.0% free SO$_3$ basis (with NaOH) were purchased from Sigma-Aldrich. All the chemicals used were of analytical grade and used without any further purification.

Methods

The IR spectra were recorded on a Perkin Elmer 1710 FTIR spectrometer with KBr disc, nichrome wire as source, lithium tantalite as detector has been used to characterize the chemical structure of graphene sheets before and after dye adsorption and the ν_{max} was expressed in cm^{-1}. The UV visible spectra of liquid samples were recorded on Perkin Elmer Lambda-35 UV/Vis spectrophotometer and the λ_{max} was expressed in nanometers. Raman spectra were recorded on in-Via Renishaw Raman spectrophotometer using a 484 nm laser source. Powder x-ray diffraction was recorded on a Bruker Discover 8 X-ray diffractometer using CuKα radiation (λ=1.54Å, 3KW) equipped with a sample stage Eulerian cradle with 6 degrees of freedom, optical system having 2D area detector and scintillation detector. The measurement was performed at room temperature in nitrogen atmosphere to minimize air scatter. The XRD spectrum of Si crystal was used as a standard to calibrate the scanning angles. The data was collected over 2θ angle range of 5<2θ<50 with a Scanning rate of 0.02°/min. TEM measurements were recorded on tungsten filament on FEI, TECNAI G^{2}T30 u-TWIN model at 50-300kV and 58x-970kx magnification to study the change in behaviour of graphene sheet before and after dye adsorption.

The sample was prepared by sonicating a pinch of powder for half an hour using methanol as a dispersing solvent, then taken on a carbon coated (50 nm thickness) Cu grid of 300 mesh and gird was dried under high vacuum pressure. Sulfonated graphene sheets were examined under SEM using JEOL JSM 6610LV with tungsten filament as source, 3µs dwell, 10.00KV voltage, 3000x magnification, 10.2mm WD. Thermogravimetric analyses were performed using Perkin Elmer, Pyris Diamond TGA, in the temperature range 30°-1000° C $\pm$ 10mg, under nitrogen atmosphere. Sonication was done on PCI^{TM} Analytics ultrasonic bath sonicator with 170 V AC - 270 V AC input voltage, 50 Hz frequency range, 45°C. Zeta potential was measured on Zeta NANO ZS Malvern Zetasizer with 10 mg/mL sensitivity. Aqueous dye solutions were prepared using deionized water.

Synthesis of graphene oxide (GO) and reduced graphene oxide (rGO)

Graphene oxide was synthesized from natural graphite powder using Hummer's method [**23**]. 5.0 g of graphite powder was added to a mixture of 5.0 g of NaNO$_3$ and 120 mL of H$_2$SO$_4$ (98%) in a 500 mL flask stirred rapidly for 30 min in an ice bath. 30 g of KMnO$_4$ was slowly added to the reaction mixture under vigorous stirring. After stirring for over 12 hours, the reaction mixture color turned to light brown. The mixture was diluted with 300 mL water under stirring, and heated to 98°C for 24 h. 100 mL of H$_2$O$_2$ (50 wt%) was then added to the mixture, and stirred for 24 h at room temperature. After cooling to room temperature, reaction mixture was rinsed and centrifuged with 5% HCl and deionized water several times until the pH became neutral, and the GO dispersion was obtained.

1g graphite oxide was dispersed in 1000 mL water by sonication for 1 h, a clear, brown dispersion of graphene oxide was formed, Na$_2$CO$_3$ (5%) was added to adjust the pH ~ 8-9. The dispersed graphene oxide was then subjected to reduction by addition of NaBH$_4$ (13.25 g, 35.04 mmol) and stirring at 70°C at reflux for 2 h. The resultant mixture was cooled to room temperature, filtered under vacuum, washed with deionized water several times, and the resultant powder was dried in vacuum at 50°C to give reduced graphene oxide.

Synthesis of sulfonated reduced graphene oxide (rGO-SO$_3$H)[24]

rGO-SO$_3$H was synthesized by the hydrothermal sulfonation of rGO using fuming sulfuric acid at 180°C. In a typical experiment, 1.0 g of rGO was added into 50 mL of fuming sulfuric acid and sonicated for 30 min. The mixture was transferred into an autoclave and the temperature was increased at the rate of 3°C/h. The vessel was heated up to 180°C for 24 h under stirring and then allowed to cool to room temperature at the same rate of 3°C/h. The resulting mixture was washed with subsequent amount of deionized water, dried at 80°C for 12 h to give sulfonated graphene.

Adsorption experiments

Different stock solutions of dye varying from 1 to 5 mg/L for Rhodamine B (RB), and 1 to 30 mg/L Methylene Blue (MB), respectively were prepared in deionized water. Aqueous solution of 50 mg/L and 100 mg/L rGO-SO$_3$H were prepared by sonication to obtain a stable colloidal solution of the adsorbent. For adsorption experiments, 100 mL of aqueous solution of adsorbent and dye solutions of required concentration were taken in a 250 mL beaker, the solution was vigorously stirred in dark. Absorbance of samples was measured at regular intervals. The dye concentrations in solution during the experiments were calculated during Lambert beers law. After the complete adsorption studies, adsorbent was filtered, dried under vacuum and used for spectroscopic characterizations. In this article, we have used three

different dyes, namely dual charged RB, negatively charged MO and positively charged MB in an aqueous solution, to study the adsorption properties of rGO-SO$_3$H.

Results and discussion

Structural characterization

Fig. 1. depicts the FT–IR spectrum of rGO-SO$_3$H. rGO-SO$_3$H shows an additional band at 1032 cm^{-1} in comparison to rGO. This band is attributed to S=O stretch [**25**], indicating the successful grafting of -SO$_3$H groups onto reduced graphene oxide. While, a low intensity band at 1705 cm^{-1} corresponds to C=O bond, attributed to some unreduced oxygen atoms on the graphene sheet. While the bands at 3544, 1600, 1161 cm^{-1} are associated with –O-H stretch in sulfonic acid groups, C=C stretch and S-O stretch in –SO$_3$, respectively.

Raman Spectrum of graphite displays a prominent G band at 1581 cm^{-1}, corresponding to the first-order scattering of the E$_{2g}$ mode [**26**]. In contrast, chemical oxidation of graphite shows peaks at 1594 and 1363 cm^{-1}, attributed to G band (the vibration of sp^2 carbon atoms in a graphitic 2D hexagonal lattice) and the D band (the vibrations of sp^3 carbon atoms arising from the defects or disorderness), respectively. While on reduction, ratio of D:G shifts from 0.89 to 1.29; which on treatment with fuming sulfuric acid, shifts to a relatively lower value of 1.19, suggesting an increase in the average size of domains by the formation of sp^3 carbons due to the incorporation of oxygen or sulfur heteroatoms during the chemical treatment [**27**]. While the two characteristic bands of r-GO at 1349, 1579 cm^{-1} shift to 1356, 1588 cm^{-1} in rGO-SO$_3$H (**Fig. 2**).

Fig. S2 shows the powder XRD pattern of rGO-SO$_3$H. After the reduction of GO by sodium borohydride, (002) peak shifts from 12.6° to 24.3°, suggesting that GO is reduced to graphene with only a few layers. After hydrothermal sulfonation, rGO-SO$_3$H exhibits a very similar XRD pattern to rGO, suggesting similar graphene layers as in rGO with a peak at 24.4°, in addition a peak at 22.2° is observed. **Fig. 3** shows the thermogravimetric curve for rGO-SO$_3$H, a higher temperature decomposition of sulfonic acid groups is observed at 250° and 557°C, respectively. These results indicate an excellent stability of rGO-SO$_3$H depicting a strong interaction of graphene with the sulfonic groups present on the basal plane.

Adsorption studies

The surface charge (zeta potential) of as-prepared sulfonated graphene sheets shows that these sheets are highly negatively charged when dispersed in water, ζ = -25.5 mV (**Fig. S3**), apparently as a result of ionization of the sulfonated groups present on graphene sheets. The excellent adsorption is the result of electrostatic and van der Waals interaction between the negatively charged sulfonated graphene sheet and positively charged dye and as revealed by the graphs it is clearly a function of i) time, ii) adsorbent dosage, iii) dye concentration, iv) pH. RB shows moderate adsorption as compared to MB, while MO shows almost negligble

adsorption. RB adsorbs to about 48%, when the dye concentration is 5 mg/L while MB adsorbs to about 98% when the dye concentration is 5 mg/L. This is due to the fact that MB is a positively charged molecule while RB has both positive as well as negative charges associated with it, hence RB does not allow a strong electrostatic interaction with sulfonated graphene, while MO being negatively charged repels the negatively charged sulfonated graphene sheet, therefore, no adsorption occurs (**Fig. 4**). (Structure of dyes used in the present studies have been provided in **Scheme 1**, ESI). Parallel behavior has been documented in literature with graphene oxide [**16**].
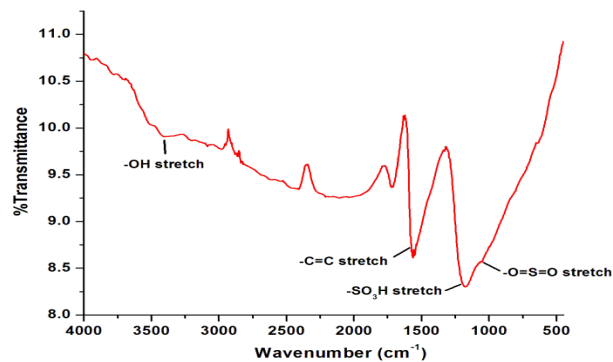
Fig. 1. FT-IR Spectra of rGO-SO$_3$H.
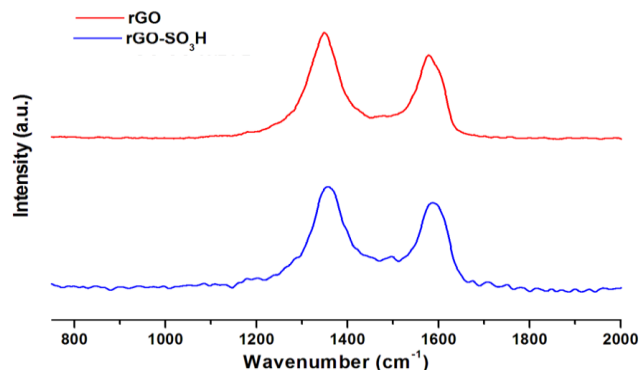
Fig. 2. Raman Spectra of rGO, rGO-SO$_3$H.
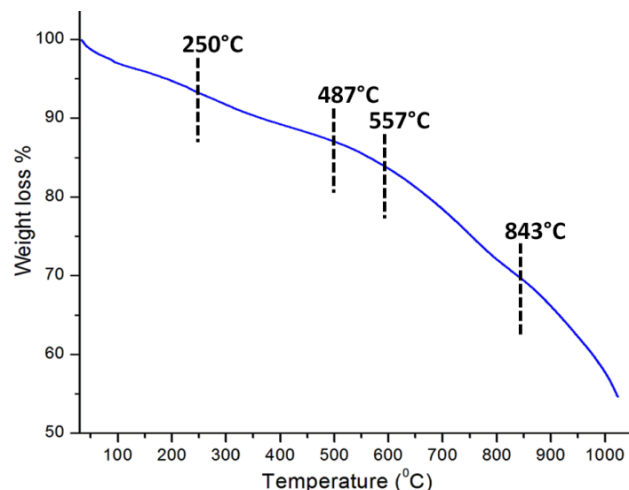
Fig. 3. Thermogravimetric analysis of rGO-SO$_3$H.

Effect of adsorbent dosage

The effect of different adsorbent dosages on RB, MB removal was studied, and the result is shown in **Fig. 4**. Obviously, the adsorption capacity improves with increase in rGO-SO₃H dosage as there is an increase in surface area and number of active sites for adsorption [**28**]. A sharp rise in RB removal efficiency from 50% to 85.5% is observed with increase in adsorbent dosage, from 0.05 to 0.10 g, respectively. RB having dual charges positive as well as negative, does not allow a strong attractive electrostatic interaction, and therefore, requires more amount of adsorbent dosage for complete removal of dye. While for MB such a steep increase is not observed by varying the adsorbent dosage. This shows strong interaction between MB and graphene even at lower graphene dosage, explaining the fast adsorption kinetics at lower concentration.

On further increase of the adsorbent dosage from 0.10 g to 0.20 g, removal efficiency decreases for MB from 99% to 82% which may be due to the fact that active sites are only partly exposed and occupied by dye at higher adsorbent dosage [**29**]. At the same adsorbent dosage, higher MB concentration acquires a higher equilibrium adsorption capacity, as larger MB concentration gradient increases the diffusion driving force of MB adsorbed by graphene [**30**].
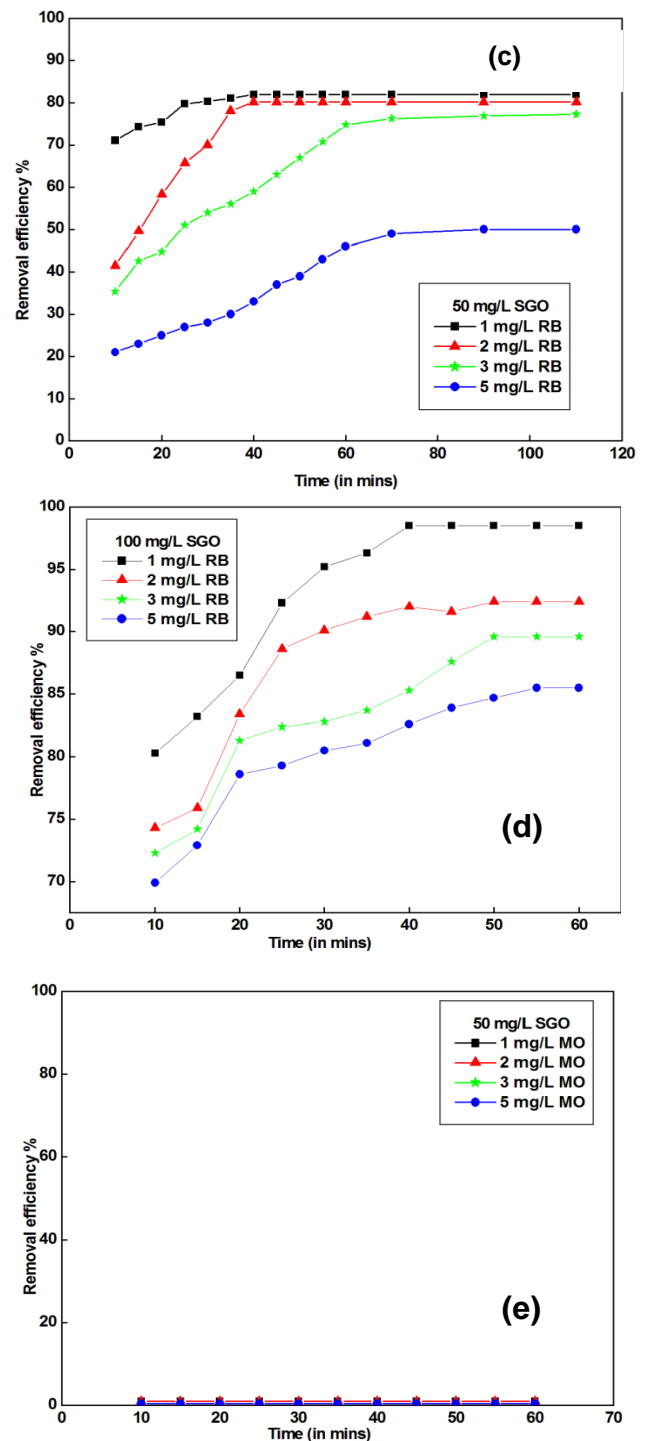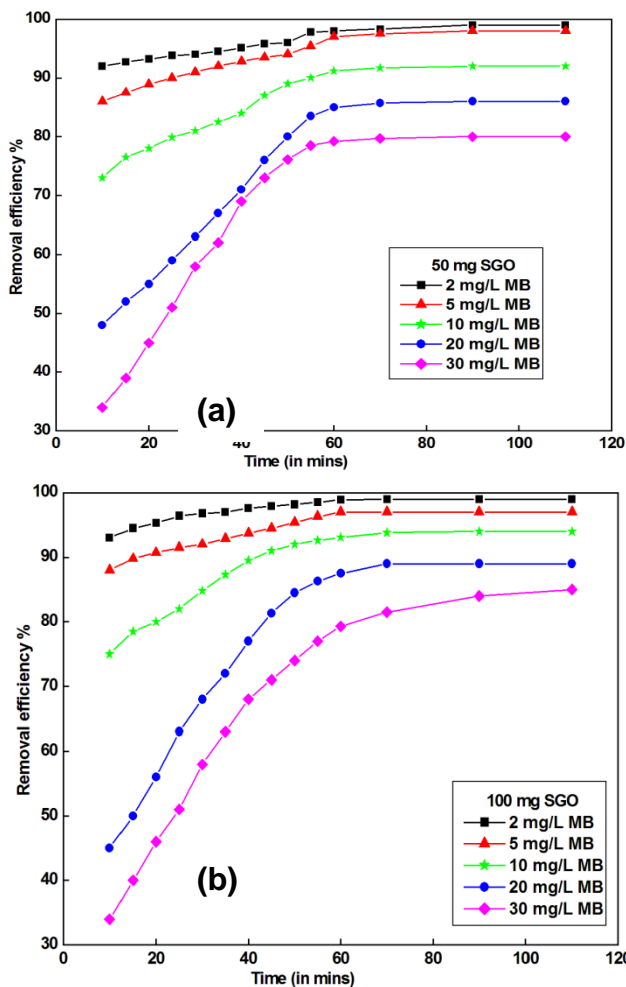
Fig. 4. Removal efficiency of a) MB, rGO-SO₃H dosage- 0.05g/L; b) MB, rGO-SO₃H dosage- 0.10g/L; c) RB, rGO-SO₃H dosage- 0.05g/L; d) RB, rGO-SO₃H dosage- 0.10g/L RB at different dye concentrations; e) MO, rGO-SO₃H dosage- 0.05g/L;

Effect of pH

Both, dye and adsorbent used in the adsorption experiment, behaves differently with variation in pH. So, it becomes important to study the variation in pH to completely understand the adsorption mechanism involved. Zeta potential of sulfonated graphene was calculated experimentally, at three different pH acidic,

neutral, and basic. The highest magnitude of ζ is obtained at pH 9 (-45.7 mV, **Fig. S4**), confirming the ionization of $-SO_3H$ groups resulting in increased negative charge on graphene sheet in alkaline medium. At a higher MB concentration of 30 mg/L, the adsorption capacity increases to 97% with increase in pH from 7 to 9, as the positive character of dye increases, and negative charges associated with the adsorbent increases, thereby, improving the electrostatic interaction between GO and MB.

While RB exists as a zwitterionic species at pH 7; and a positively charged species at pH 2. Hence, the adsorption capacity is observed maximum for RB at pH 2, and lowest at pH 7. The complexity in adsorption at pH 7 may be attributed to the dual charge associated with the dye molecule. Similar pH-regulated adsorption behavior has been observed for other carbon adsorbents.[31] Based on adsorption capacity the optimized pH values are 10 for MB and 2 for RB, respectively (**Fig. 5**).
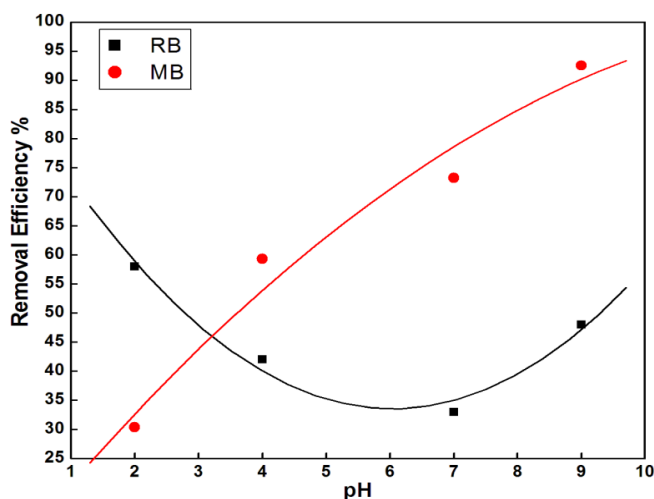
Fig. 5. Dye removal efficiency with pH for RB, MB on rGO-SO$_3$H

Equilibrium adsorption isotherm

Freundlich and Langmuir are the mathematical models used frequently to fit the experimental data for describing equilibrium studies for the adsorption of dyes on solid surfaces. In this work, experimental data for batch adsorption isotherm experiments by varying the amount of adsorbent with MB, RB dyes were applied to both models. The Langmuir model assumes the adsorption to be a homogenous phenomenon and that no interaction occurs between adsorbates in the plane of the surface.[32] The Langmuir isotherm equation is as follows:

$$\frac{C_e}{q_e} = \frac{C_e}{q_m} + \frac{1}{k_L q_m}$$

where C_e is the equilibrium concentration of the solution (mg/L), q_m is the maximum adsorption capacity (mg/g), k_L is a Langmuir constant related to the affinity of the binding sites and energy of adsorption (L/g). A linear plot of C_e/q_e vs q_e indicates adsorption process follows Langmuir isotherm, q_{max}, k_L was evaluated from the slope and intercept, respectively. The adsorption process was

also characterized by Vermeulan criteria[32] associated with the Langmuir isotherm. A dimensionless constant describes Vermeulan criteria, and is given by

$$R_L = \frac{1}{1 + K_L C_O}$$

The value of R_L indicates the adsorption process to be either unfavorable ($R_L > 1$), linear ($R_L = 1$), favorable ($0 < R_L < 1$), or irreversible ($R_L = 0$).

The maximum capacity of the adsorbent used for MB was found to be 564.971 mg/g, which is higher than the reported values of exfoliated graphene oxide 350 mg/g[33], and graphene 153.85 mg/g [**28**]. The value of R_L was found to be 0.045 for MB, therefore, indicates the adsorption to be favorable process.

The Freundlich adsorption equation based on adsorption on a heterogeneous surface is given by:

$$\log q_e = \log k_f + \frac{1}{n_f} \log C_e$$

where k_f is a Freundlich constant related to adsorption capacity (L/g), and $1/n_f$ is an empirical parameter related to adsorption intensity. A straight line was obtained when Log q_e was plotted against Log C_e and n and k_F could be evaluated from the slope and intercept. **Table 1** summarizes the corresponding constants for dyes on different isotherm, while **Fig. 6** shows the adsorption isotherm graphs.

According to the coefficients of determination, adsorption of MB fits Langmuir as well as Freundlich model equally well. However, RB follows the Freundlich behavior better than Langmuir behavior.
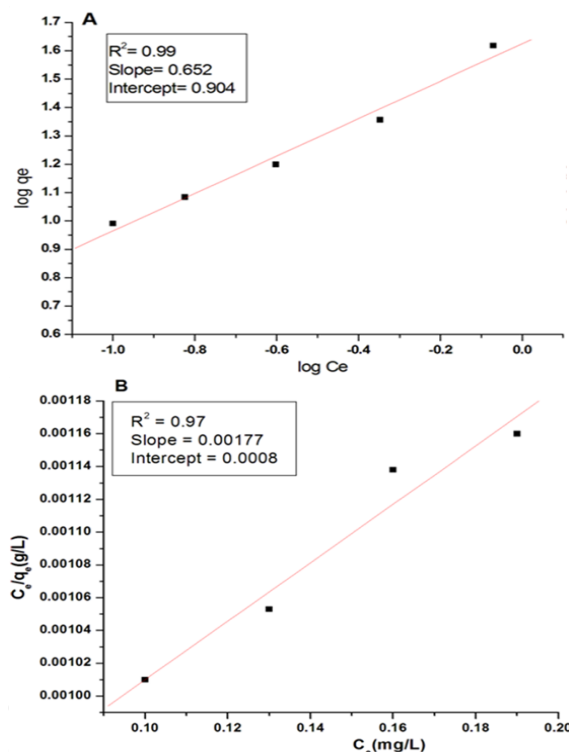
Fig. 6. (a) Freundlich adsorption isotherm for RB; (b) Langmuir adsorption isotherm for MB on rGO-SO$_3$H.

Dye-adsorbent interaction

Spectral analyses were performed on the graphene sheets before, and after adsorption of dye to understand the mechanism of adsorption process. Research groups have reported changes in the electronic structure of graphene due to interaction between electron withdrawing and electron donating groups present on graphene which can be elaborated from the Raman spectra. Dye composites show blue shifts in D and G bands 1354, 1586 cm^{-1} (rGO-SO$_3$H/RB), 1351, 1583 cm^{-1} (rGO-SO$_3$H/MB) in comparison to rGO-SO$_3$H (**Fig. 7b**). Based on the variation in G band position in Raman spectral data, it can be concluded that the charge transfer is from rGO-SO$_3$H to dye molecule (RB or MB). Similar observations on graphene and carbon nanotubes have been reported by Das and Voggu research groups [**34,35**]. While no such change is observed in the spectrum of rGO-SO$_3$H/MO with the D, G bands at 1356, 1587 cm^{-1}.

The FT-IR spectrum was also analyzed to understand the changes observed between the graphene-dye composite and graphene sheet. rGO-SO$_3$H/dye composite depicts a decrease in the intensity of –OH in sulfonic acid group observed at 3544 cm^{-1} and a new band appears at 2336cm^{-1}. The decrease in intensity may be attributed to the electrostatic interactions of nitrogen atom and sulphur atom of RB and MB, respectively, with the hydroxyl groups present in –SO$_3$H associated with the graphene sheets (**Fig. 7a**). Such changes were not observed for rGO-SO$_3$H/MO composite and hence no adsorption was observed for negatively charged dye. TEM analyses indicate the sheets to be more crumpled, folded after interaction with RB (**Fig. 7c, d**).

Based on the above data, it is postulated that rGO-SO$_3$H/MB is electrostatic in nature while rGO-SO$_3$H/RB interacts via electrostatic as well as van der Waals type. This type of electrostatic interaction for the adsorption of cationic organic dyes on GO have been reported by Ramesha et.al.[**36**], Dass et.al.[**37**], Bradder et.al[**33**].
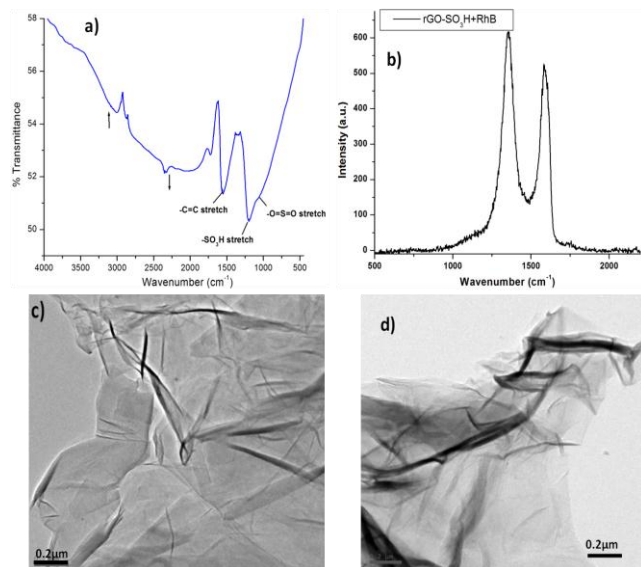
Fig. 7. (a) FTIR spectrum of; (b) Raman spectrum; TEM Analysis of (c) rGO-SO$_3$H, d) rGO-SO$_3$H/RB composite.

Table 1. Adsorption isotherm for different dyes.

	Langmuir Isotherm				Freundlich isotherm		
	q$_m$ (mg/g)	k$_L$ (L/mg)	R^2	R$_L$	k$_f$ (mg/g)	n$_f$	R^2
RB	76.68	1.18	0.88	0.144	8.016	1.53	0.99
MB	564.97	2.12	0.97	0.045	90.15	1.11	0.97

Table 2. Variation in the G band in rGO-SO$_3$H/dye composite.

Material Composite	**G Band variation (cm^{-1})**
rGO-SO$_3$H	1588
rGO-SO$_3$H/RB	1586
rGO-SO$_3$H/MB	1583
rGO-SO$_3$H/MO	1587

Conclusion

This present study explains sulfonated graphene as a better adsorbent for organic cationic dyes with a maximum adsorbent capacity of 564.971 mg/g in comparison with graphene oxide and reduced graphene oxide. The adsorption was found to be dependent on adsorbent dosage, dye concentration, contact time, and pH. The physical adsorption as probed by Raman and FT-IR is mainly due to electrostatic interactions of oppositely charged adsorbate-adsorbent species in Methylene Blue while the π−π interactions dominate in Rhodamine B. The adsorption conditions can be tuned to maximize the removal efficiency for various dye molecules.

Author's contributions

Conceived the plan: Smriti Arora, Ritika Nagpal, Sweta Mishra; Performed the experiments: Smriti Arora, Ritika Nagpal; Data analysis: Smriti Arora, Ritika Nagpal; Manuscript Preparation: Smriti Arora, Ritika Nagpal, SMS Chauhan. Authors have no competing financial interests.

Supporting information

Supporting informations are available from VBRI Press.

References

1. Ayad, M. M.; El-Nasr, A. A. *J. Phys. Chem. C* **2010**, *114*, 14377.
    DOI: 10.1021/jp103780w
2. Verma, A. K.; Dash, R. R.; Bhunia, P. *J. Environ. Manage*. **2012**, *93*, 154.
    DOI: 10.1016/j.jenvman.2011.09.012
3. Malik, P. K. *Dyes Pigm.* **2003**, *56*, 239.
    DOI: 10.1016/S0143-7208(02)00159-6
4. Ghaedi, M.; Golestani Nasab, A.; Khodadoust, S.; Rajabi, M.; Azizian, S. *J. Ind. Eng. Chem.* **2014**, *20(4)*, 2317.
    DOI: 10.1016/j.jiec.2013.10.007

5. Arami, M.; Limaee, N. Y.; Mahmoodi, N. M. Tabrizi, N. S. *J. Colloid Interface Sci..* **2005**, *288*, 371.
DOI: 10.1016/j.jcis.2005.03.020

6. Bhattacharya, K.G.; Sharma, A . *Dyes Pigm.* **2005**, *65*, 51.
DOI: 10.1016/j.dyepig.2004.06.016

7. Gupta, V.K.; Suhas, I.A.; Saini, V.K. *Ind. Eng. Chem. Res.* **2004**, *43*, 1740.
DOI: 10.1021/ie034218g

8. Mittal, A.; Kurup, K.L.; Gupta, V.K. *J. Hazard. Mater.* **2005**, *117*, 171.
DOI: 10.1016/j.jhazmat.2009.06.012

9. Grag, V.K.C.; Amita, M.; Kumar, R.; Gupta, R. *Dyes Pigm.* **2004**, *63*, 243.
DOI: 10.1016/j.dyepig.2004.03.005

10. Mahanta, D.; Madras, G.; Radhakrishnan, S.; Patil, S. *J. Phys. Chem. B* **2009**, *113*, 2293.
DOI: 10.1021/jp809796e

11. Kant, R. *J. Water Resour. Prot.* **2012**, *4(2)*, 93.
DOI: 10.4236/jwarp.2012.42011

12. Dimiev, A. M.; Eigler, S.; Graphene Oxide: Fundamentals and Applications; Wiley: USA, **2016.**

13. Upadhyay, R. K.; Soin, N.; Roy, S. S. *RSC Adv.* **2014**, *4*, 3823.
DOI: 10.1039/C3RA45013A

14. Ramesha, G. K.; Kumara, A. V.; Muralidhara, H. B.; Sampath, S. *J. Colloid Interface Sci.* **2011**, *361*, 270.
DOI: 10.1016/j.jcis.2011.05.050

15. Mishra, A.K.; Ramaprabhu, S. *J. Hazard. Mater.* **2011**, *185*, 322.
DOI: 10.1016/j.jhazmat.2010.09.037

16. Yang, S.T.; Chang, Y.; Wang, H.; Liu, G.; Chen, S.; Wang, Y.; Liu, Y.; Cao, A. *J. Colloid Sci.* **2010**, *351*, 122.
DOI: 10.1016/j.jcis.2010.07.042

17. Balapanuru, J.; Yang, J.; Xiao, S.; Bao, Q.; Jahan, M.; Polavarapu, L.; Wei, J.; Xu, Q.; Loh, K.P. *Angew. Chem., Int. Ed.* **2010**, *49*, 6549.
DOI: 10.1002/anie.201001004

18. Yusuf, M.; Elfghi, F. M.; Zaidi, S. A.; Abdullah, E. C.; Khan, M. A. *RSC Adv.* **2015**, *5*, 50392.
DOI: 10.1039/C5RA07223A

19. Gul, K.; Sohni, S.; Waqar, M.; Ahmad, F.; Norulaini, N. A. N.; Omar A.K. *Carbohydrate Polymers*, **2016**, *152*, 520.
DOI: 10.1016/j.carbpol.2016.06.045

20. Scalese, S.; Nicotera, I.; D'Angelo, D.; Filice, S.; Libertino, S.; Simari, C.; Dimos, K.; Privitera, V. *New J. Chem.*, **2016**, *40*, 3654.
DOI: 10.1039/C5NJ03096J

21. Mishra, S.; Arora, S.; Nagpal, R.; Chauhan, S.M.S.; *J. Chem. Sci.*, **2015**, *126*, 1729.
DOI: 10.1007/s12039-014-0731-8

22. Zhang, L.; Bao, Z.; Yu, X.; Dai, P.; Zhu, J.; Wu, M.; Li, G.; Liu, X.; Sun, Z.; Chen, C. *ACS Appl. Mater. Interfaces*, **2016**, *8* , 6431.
DOI: 10.1021/acsami.5b11292

23. Tang , L.; Chang , H.; Liu, Y.; Li, J. *Adv. Funct. Mater.* **2012**, *22*, 3083.
DOI: 10.1002/adfm.201102892

24. Liu, F.; Sun, J.; Zhu, L.; Meng, X.; Qi, C.; Xiao, F. S. *J. Mater. Chem.* **2012**, *22*, 5495.
DOI: 10.1039/C2JM16608A

25. Suganuma, S.; Nakajima, K.; Kitano, M.; Kato, H.; Tamura, A.; Kondo, H.; Yanagawa, Hayashi, S.; Hara, M. *Microporous Mesoporous Mater.* **2011**, *143*, 443.
DOI: 10.1016/j.micromeso.2011.03.028

26. Tuinstra, F.; Koenig, J. L. *J. Chem. Phys.* **1970**, *53*, 1126.
DOI: 10.1063/1.1674108

27. (a) Kudin, K. N.; Ozbas, B.; Schniepp, H. C.; Prud'homme, R. K.; Aksay, I. A.; Car, R. *Nano Lett.* **2008**, *8 (1)*, 36.
DOI: 10.1021/nl071822y
(b) Ramesha, G. K.; Sampath, S. *J. Phys. Chem. C* **2009**, *113* (19), 7985.
DOI: 10.1021/jp811377n

28. Liu, T.; Yanhui Li, Y.; Dua, Q.; Sun, J.; Jiao, Y.; Yang, G.; Wang, Z.; Xia, Y.; Zhang, W.; Wang, K.; Zhu, H.; Wuc, D. *Colloids Surf., B* **2012**, *90*, 197.
DOI: 10.1016/j.colsurfb.2011.10.019

29. Li, Y.; Dua, Q.; Wang, X.; Zhanga, P.; Wang, D.; Wanga, Z.; Xiaa, Y. *J. Hazard. Mater.* **2010**, *183*, 583.
DOI: 10.1016/j.jhazmat.2010.07.063

30. Yao, Y.; Xu, F.; Chen, M.; Xu, Z.; Zhu, Z. *Bioresour. Technol.* **2010**, *101*, 3040.
DOI: 10.1016/j.biortech.2009.12.042

31. Rodriguez, A.; Gracia, J.; Ovejero, G.; Mestanza, M. *J. Hazard. Mater.* **2009**, *172*, 1311.
DOI: 10.1016/j.jhazmat.2009.07.138

32. Ai, L.; Li, L. M.; Li, L. *J. Chem. Eng. Data* **2011**, *56*, 3475.
DOI: 10.1021/je200536h

33. Bradder, P.; Ling, S. K.; Wang, S.; Liu, S. *J. Chem. Eng. Data* **2011**, *56(1)*, 138.
DOI: 10.1021/je101049g

34. Das, B.; Voggu, R.; Rout, C.S.; Rao, C.N.R. *Chem. Commun.* **2008**, 5155.
DOI: 10.1039/B808955H

35. Voggu, R.; Rout, C.S.; Franklin, A.D.; Fisher, T.S.; Rao, C.N.R. *J. Phys. Chem. C* **2008**, *112*, 13053.
DOI: 10.1021/jp805136e

36. Ramesha, G. K.; Kumara, A. V.; Muralidhara, H. B.; Sampath, S. *J. Colloid Interface Sci.* **2011**, *361*, 270.
DOI: 10.1016/j.jcis.2011.05.050

37. Sharma, P.; Das, M. R. *J. Chem. Eng. Data* **2013**, *58*, 151.
DOI: 10.1021/je301020n